

MIGRATION OF PLANETS EMBEDDED IN A CIRCUMSTELLAR DISK

BENJAMIN C. BROMLEY¹ AND SCOTT J. KENYON²

¹ Department of Physics & Astronomy, University of Utah, 115 S 1400 E, Rm 201, Salt Lake City, UT 84112, USA; bromley@physics.utah.edu

² Smithsonian Astrophysical Observatory, 60 Garden Street, Cambridge, MA 02138, USA; skenyon@cfa.harvard.edu

Received 2011 January 26; accepted 2011 April 13; published 2011 June 10

ABSTRACT

Planetary migration poses a serious challenge to theories of planet formation. In gaseous and planetesimal disks, migration can remove planets as quickly as they form. To explore migration in a planetesimal disk, we combine analytic and numerical approaches. After deriving general analytic migration rates for isolated planets, we use N -body simulations to confirm these results for fast and slow migration modes. Migration rates scale as m^{-1} (for massive planets) and $(1 + (e_H/3)^3)^{-1}$, where m is the mass of a planet and e_H is the eccentricity of the background planetesimals in Hill units. When multiple planets stir the disk, our simulations yield the new result that large-scale migration ceases. Thus, growing planets do not migrate through planetesimal disks. To extend these results to migration in gaseous disks, we compare physical interactions and rates. Although migration through a gaseous disk is an important issue for the formation of gas giants, we conclude that migration has little impact on the formation of terrestrial planets.

Key words: circumstellar matter – planetary systems – planet-disk interactions – planets and satellites: formation

Online-only material: animation, color figures

1. INTRODUCTION

Migration is an important physical process in planet formation (e.g., Lin & Papaloizou 1986; Ward 1997; Artymowicz 2004; Levison et al. 2007; Papaloizou et al. 2007; Kirsh et al. 2009; D’Angelo et al. 2010; Lubow & Ida 2010, and references therein). Based on analytic theory and detailed numerical simulations, several modes of interaction between growing planets and density perturbations within a disk of gas or within a disk of planetesimals produce secular evolution of the orbital semi-major axis, eccentricity, and inclination of a planet. For planets with masses exceeding $\sim 0.1 M_{\oplus}$, derived migration rates have a broad range, $\sim 10^{-7}$ – 10^{-4} AU yr⁻¹. On typical timescales of 0.1–1 Myr, planets can migrate through the entire disk.

To explain the frequency of ice giant and gas giant planets close to their parent stars, migration is essential (Lin et al. 1996; Marzari & Weidenschilling 2002; Ida & Lin 2004; Alibert et al. 2004). Although there are significant selection biases, most known exoplanets have semimajor axes, $a \lesssim 0.1$ –1 AU (data from exoplanet.org and exoplanet.eu). Protostellar disks probably do not have enough mass to produce ice giants or gas giants so close to their parent stars (e.g., Bodenheimer et al. 2000; Kornet et al. 2002). Once these planets form farther out in the disk, however, they can slowly migrate inward to close-in orbits around their parent stars (e.g., Ida & Lin 2005; Armitage 2007; Thommes et al. 2008; Mordasini et al. 2009).

Migration may also explain the orbital architecture of the solar system. Observations of the dynamical structure of the Kuiper Belt suggest that Neptune migrated outward from its likely birthplace (Malhotra 1993; Hahn & Malhotra 1999). Other evidence suggests that the four gas giants formed in a more compact configuration and then migrated outward (e.g., Thommes et al. 2002; Tsiganis et al. 2005; Morbidelli et al. 2008).

Despite these successes, migration is a great challenge for theories of planet formation. In the current picture, terrestrial planets and the cores of at least some gas giant planets form

by a coagulation process, where lower mass objects collide and merge into larger objects. Early on, migration timescales are long. Without straying too far from their birthplaces, protoplanets undergo runaway growth—where a few of the largest objects grow much much faster than other objects—and then oligarchic growth—where these largest objects grow more slowly but still faster than much less massive objects (e.g., Kokubo & Ida 1998; Goldreich et al. 2004; Kenyon & Bromley 2010, and references therein). As planets begin to reach masses of $\sim 0.1 M_{\oplus}$, however, collision times become longer than migration times. Thus, theory predicts that the final building blocks of planets migrate into the central star before they reach the mass of the Earth (Lin & Papaloizou 1979; Goldreich & Tremaine 1980; Artymowicz 1993b; Ward 1997; Masset & Papaloizou 2003; Ida & Lin 2008).

Migration is also a severe problem for the formation of ice giant and gas giant planets. Once ice giants or gas giants are fully formed, migration can produce the close-in giant planets observed around nearby stars (Ida & Lin 2005). However, theory predicts a more rapid migration of the lower mass building blocks of ice and gas giants (Ward 1997; Masset & Papaloizou 2003; Ida & Lin 2008; Pepliński et al. 2008a). In the standard theory, these lower mass planets migrate too fast to produce ice or gas giants. Solving this problem is a central issue in planet formation theories.

Theories of migration generally focus on isolated planets interacting with the disk (see Papaloizou et al. 2007, and references therein). Recent attempts to understand how real planets avoid migration concentrate on the physics of this isolated interaction, including disk dynamics (Masset et al. 2006; Pepliński et al. 2008a; Paardekooper & Papaloizou 2009a, 2009b), magnetic fields (Terquem 2003), orbital eccentricity (Papaloizou & Larwood 2000), disk thermodynamics (Kley & Crida 2008; Paardekooper & Mellema 2006b; Paardekooper & Papaloizou 2008; Kley et al. 2009; Paardekooper et al. 2010, 2011), and turbulence (Nelson & Papaloizou 2004; Adams & Bloch 2009). While any or all of these processes may reduce migration rates to acceptable levels, growing protoplanets are

not isolated. Tightly packed protoplanets probably perturb the disk differently than systems of widely spaced protoplanets. Thus, migration rates may depend as much on the local density of protoplanets as on the scale of specific interactions between an isolated planet and the disk.

Here, we consider how migration operates in systems of multiple planets. Building on previous work (e.g., Malhotra 1993; Hahn & Malhotra 1999; Levison et al. 2007; Kirsh et al. 2009), we examine migration in disks of planetesimals with single planets (Sections 2.1–2.3) and multiple planets (Sections 2.4 and 2.5). These results show that migration is rarely important in planet-forming disks of planetesimals. In Section 3, we then explore the implications of our results for (inviscid) planetesimals embedded in (viscous) gaseous disks. If our assumptions about viscous disks are valid, migration is rarely important during terrestrial planet formation. However, it is still an important issue in the formation of ice giant and gas giant planets. We conclude with a brief summary and suggestions for further study in Section 4.

2. PLANETARY MIGRATION IN A PLANETESIMAL DISK

Planets migrate through a planetesimal disk as a result of pairwise exchange of angular momentum between the planet and individual disk particles (Lin & Papaloizou 1979; Goldreich & Tremaine 1979, 1980; Artymowicz 1993a). An important distance scale for this exchange is the planet’s Hill radius,

$$r_H = a \left(\frac{m}{3M} \right)^{1/3}, \quad (1)$$

where a is the planet’s semimajor axis, m is its mass, and M is the mass of the central star. If the semimajor axis of a disk particle is $a + \delta r$, where δr is its orbital separation from the planet, then a passing encounter changes the planet’s semimajor axis by

$$\delta \tilde{a} \approx g(x) \frac{r_H}{m}, \quad (2)$$

where $x = \delta r/r_H$, $g(x)$ is a function that depends on the geometric shape of the planetesimal’s trajectory relative to the planet, and the tilde symbol indicates a change in orbital distance per unit planetesimal mass. Equation (2) asserts that the dimensions of a particle’s trajectory near the planet scale as r_H ; the planet’s recoil conserves momentum and must depend on $1/m$.

To calculate the trajectory function $g(x)$, we consider nearby particles in the co-orbital zone of the planet and more distant particles in the small-angle limit. Planetesimals in the co-orbital zone, with $|\delta r| \lesssim 2r_H$, follow almost the same orbit as the planet but get pushed gently toward and away from it on horseshoe orbits (Dermott & Murray 1981). More distant planetesimals at $|\delta r| \gtrsim 4r_H$ stream by the planet and experience small-angle scattering relative to their Keplerian path. The trajectory function in these two cases is

$$g(x) = \begin{cases} 2x & (|x| \lesssim 2; \text{co-orbital}), \\ -32x^{-5} & (|x| \gtrsim 4; \text{small-angle scattering}). \end{cases} \quad (3)$$

The co-orbital zone result follows from conservation of energy. When the pair’s relative speed is much greater than the planet’s escape velocity at closest approach, the small-angle expression for larger separations follows from two-body scattering theory (Lin & Papaloizou 1979).

To illustrate this scaling property, we consider a set of numerical simulations of planetesimals on circular orbits close

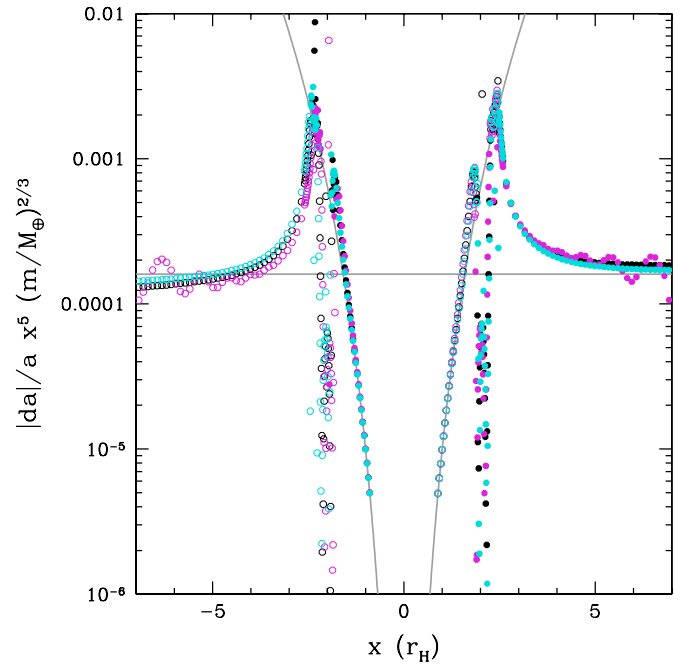


Figure 1. Derived change in semimajor axis (da) of a planet after an encounter with a planetesimal as a function of their initial orbital separation (x) in Hill units. Objects start 180° out of phase on circular orbits, with the planet at $a = 1$ AU from the central star ($1 M_\odot$); da (scaled by x^5 in the plot) is the resulting change in a after one synodic period. Planetesimals have masses of $5 \times 10^{-4} M_\oplus$. Colors distinguish planet mass: $m = 0.125 M_\oplus$ (cyan), $1 M_\oplus$ (black), and $8 M_\oplus$ (magenta); symbol attribute identifies the sense of migration: outward (open) or inward (filled). The scaling of da with m agrees with Equation (2). The steep curves are theoretical predictions for the co-orbital zone (Equation (3)); the horizontal line is from small-angle scattering theory.

(A color version of this figure is available in the online journal.)

to a much more massive planet (similar to Figure 5 in Ida et al. 2000). Bromley & Kenyon (2006) describe our orbit integrator (see also Bromley & Kenyon 2011). The planet and the planetesimal start 180° out of phase on circular orbits at distances a (planet) and $a + \delta r$ (planetesimal) from the central $1 M_\odot$ central star. We measure da as the change in a when the planet and the planetesimal complete a single synodic orbit.

Our results agree very well with the scaling law (Figure 1). For three planet masses, scaled according to Equation (2), the calculated $\delta \tilde{a}$ tracks the prediction well for co-orbital particles ($|x| \lesssim 1.8$) and distant particles in the small-angle limit ($|x| \gtrsim 4$). This scaling law begins to break down when the mass of the planet approaches the mass of the central star, but our results lend strong support for the “universality” of the trajectory function $g(x)$.

Orbital separations too distant for co-orbital encounters and too close for small-angle scattering encounters lead to chaotic scattering. A formal outer boundary for this limit is

$$r_{\text{xing}} = 2\sqrt{3}r_H. \quad (4)$$

Outside this separation, there is an energy–angular-momentum barrier that prevents chaotic orbit crossings for bodies on initially circular orbits (Gladman 1993). The inner boundary is the edge of the co-orbital region; thus, we adopt a chaotic zone with $1.8r_H \lesssim \delta r \lesssim 3.5r_H$. Figure 1 shows that particles in this region do not follow a simple trajectory function as in Equation (3).

The trajectory of a particle passing by a planet depends on whether the particle’s approach is inside or outside the orbit of

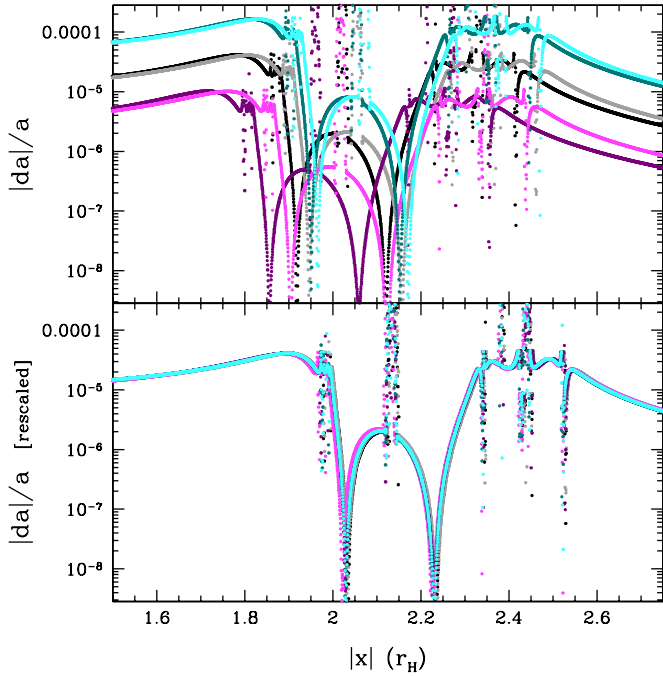


Figure 2. As in Figure 1 for planetesimal orbits in the chaotic regime. Colors indicate mass for 0.125 (cyan), 1 (gray/black), and 5 (*m*_⊕) (*m*_⊕) planets. The darker (lighter) shades indicate interactions with planetesimals that are initially inside (outside) of the planet’s orbit. The lower panel shows the alignment of these curves after applying the scaling relation in Equation (5), which transforms *da* into the “universal” trajectory function, $g(x)r_H/m$.

(A color version of this figure is available in the online journal.)

the planet. This asymmetry is evident in Figure 1, where particles with large negative *x* have smaller $|da|$ than particles with large positive *x*. We can correct Equation (2) for this property of the orbits using a first-order Taylor series expansion:

$$d\tilde{a} \approx \left[g(x) - \frac{\beta x^2 r_H}{a} \frac{dg}{dx} \right] \frac{r_H}{m}. \quad (5)$$

From numerical simulations, we estimate $\beta = 3/8$ in the chaotic regime and $\beta = 9/20$ in the small-angle limit. Figure 2 shows $\delta\tilde{a}$ in simulations with various planet masses and with planetesimals that start inside and outside of the planet’s orbit. After normalizing our results using Equation (5), these traces yield nearly the same “universal” curve $g(x)$.

2.1. Theoretical Migration Rates

To estimate a migration rate from this formalism, we need a relation for the encounter frequency. Although this frequency can vary substantially between consecutive passes of the same planetesimal (Kirsh et al. 2009), a good characteristic number is the inverse of the synodic period,

$$\frac{1}{T_{\text{syn}}} \approx \frac{3|\delta r|}{2aT} \left(1 - \frac{5\delta r}{4a} \right) \quad (6)$$

where $T = 2\pi a^{3/2}/(GM)^{1/2}$ is the orbital period of the planet. The product of this expression and Equation (5) yields a migration rate per unit mass of planetesimals.

Extending this rate to a disk of planetesimals passing by the planet requires a surface density distribution for the disk. We adopt a smooth surface density Σ over an annulus with area $2\pi r \delta r$. Expanding all terms with $r = a + \delta r$ in a Taylor series,

keeping only first-order terms in δr , and converting to a form with *x* and *dx* yields an integral for the migration rate:

$$\frac{da}{dt} = \frac{\pi a^2 \Sigma}{M} \frac{a}{T} \int |x| g(x) dx \times \left[1 + \left(\frac{a}{\Sigma} \frac{d\Sigma}{da} - \beta \frac{x}{g} \frac{dg}{dx} - \frac{1}{4} \right) \frac{r_H x}{a} \right], \quad (7)$$

where $g(x)$ is from Equation (3). The surface density Σ is often parameterized as a power law, with

$$\Sigma(a) = \Sigma_0 \left(\frac{a}{a_0} \right)^n, \quad (8)$$

and $n = 1-1.5$. We use this form of Σ throughout, setting $n = 1$, $a_0 = 1$ AU, and $\Sigma_0 = 30$ g cm⁻² unless otherwise specified.

2.1.1. Migration from Small-angle Scattering

To understand the implications of Equation (7), we consider several simple cases. For distant encounters between a planet and material in a power-law disk at separations $|x| \gtrsim 4$, we derive the migration rate from Equation (7) with $g(x) = -32/x^5$ and $\beta = 9/20$

$$\frac{da}{dt} = -\frac{32\pi a^2 \Sigma}{M} \frac{a}{T} \int \text{sgn}(x) \frac{dx}{x^4} \times \left[1 + (2-n) \frac{r_H x}{a} \right] \quad (|x| \gtrsim 4), \quad (9)$$

where Σ is evaluated at the planet’s position. If a planet lies embedded in a large disk where the inner (outer) radii are small (large) compared to the planet’s semimajor axis, the first term in the square brackets vanishes; the migration rate then depends weakly on planet mass through the second term involving r_H (see also Ida et al. 2000; Kirsh et al. 2009). If a planet lies on the inside or the outside of the disk, the first term dominates.

Provided it is no closer than r_{xing} from the planet, Equation (9) predicts that a disk situated just inside or outside a planet’s orbit is repulsive. To confirm this behavior numerically, we use an *N*-body code that evolves massive planets, along with massive planetesimals that interact with the planets but not with each other (i.e., the disks are not self-gravitating; see Bromley & Kenyon 2011). For example, a 100 *M*_⊕, $n = 1$ power-law disk consisting of 2×10^5 equal-mass particles between 26.5 AU and 35.5 AU pushes a 0.3 *M*_⊕ planet at 25 AU inward with a speed of 0.012 AU/10 kyr (Equation (9)). Simulations of 100 planetary orbits yields 0.0117 ± 0.004 AU/10 kyr. Tests with a disk inside the planet’s orbit confirm that the planet migrates outward, as expected from Equation (9).

With this formalism, we can consider an idealized example of the migration of a planet nestled between two equal-mass annuli of planetesimals. For a surface density $\Sigma \propto a^{-1}$ and spacing between the planet and each annulus of $\delta r > r_{\text{xing}}$, Equation (9) predicts a net inward migration. For an Earth-mass planet at 25 AU, between two 0.5 AU annuli centered on 23 AU and 27 AU, with 50 *M*_⊕ apiece, the theoretical migration rate is -0.019 AU/10 kyr. Although the planet eventually migrates through the gap into the inner disk of planetesimals, our numerical simulation using 1/600 *M*_⊕ planetesimals yields a migration rate of -0.025 ± 0.002 AU/10 kyr. In this simulation, migration leads to more interactions with the inner disk of planetesimals than predicted by the analytic theory; still, this numerical result agrees reasonably well with the analytic prediction.

In these examples, the gap between the planet and the disk spans the chaotic and co-orbital zones. In small-angle scattering, migration is fairly small, $\sim 1\text{--}2$ AU Myr $^{-1}$. For typical growth times of $\sim 1\text{--}3$ Myr (e.g., Kenyon & Bromley 2006; Bromley & Kenyon 2011), planets migrate through a small fraction of the disk.

2.1.2. Fast Migration

For a planet embedded in a planetesimal disk, the co-orbital zone is much more important than the small-angle scattering regime (Ward 1991; Ida et al. 2000). Over a complete libration period of a horseshoe orbit, there is no net migration of a planet responding to a planetesimal. If the planet is already moving radially inward (or outward) on a timescale shorter than the libration period, the situation is different. The planet can then pull itself along, continually exchanging places with the co-orbital material in its path. When this mechanism works, it is efficient and relatively fast.

Simulations performed with our code and other codes (Ida et al. 2000; Kirsh et al. 2009) suggest that fast migration can be inward or outward. Kirsh et al. (2009) identify a strong preference for inward migration. Our calculations confirm this conclusion; more massive planets also seem to migrate inward more often than less massive planets. We speculate that inward migration dominates in most simulations from the gentle inward push of the weakly scattered disk, whose influence on a planet increases with m .

The fast migration rate da_{fast}/dt follows from integrating Equation (7) over the half of the co-orbital zone that a planet traverses. We adopt this half-width as $\delta r = X_{\text{co}} r_{\text{H}}$, with $X_{\text{co}} = 1.8$. However, fast migration occurs only if the rate allows a planet to clear the co-orbital zone during the libration period of the planetesimal at the zone's edge. Otherwise, the planetesimal orbits back and provides a counter-torque before the planet migrates away. Large planetary masses have large co-orbital zones that are hard to traverse in a single libration period. Thus, this requirement sets a mass limit on fast migration,

$$m_{\text{fast}} \approx 4.0 \left(\frac{2\pi a^2 \Sigma X_{\text{co}}}{3M \cdot 1.8} \right)^{3/2} M. \quad (10)$$

In a disk with a surface density of 30 g cm^{-2} at 1 AU from a solar mass central star, this limit is $m_{\text{fast}} \approx 0.025 M_{\oplus}$.

To estimate the migration rate for planets more massive than m_{fast} , we consider a simple model. Fast migration relies on a planet crossing the co-orbital zone, with size $\delta r \sim r_{\text{H}}$, within a typical synodic period of an orbiting planetesimal. When $m > m_{\text{fast}}$, the co-orbital zone is too large for the planet to cross in a single synodic period. Thus, a fraction of the material in the co-orbital zone has multiple interactions with the planet, slowing the migration rate. This fraction increases with m ; thus, more massive planets migrate more slowly. To quantify this statement, we define $X_{\text{co,fast}}$ as the size of the co-orbital zone for a planet with $m = m_{\text{fast}}$. Planets with $m > m_{\text{fast}}$ have larger co-orbital zones, with $X_{\text{co}} > X_{\text{co,fast}}$. For these planets, we assume that planetesimals within a distance $X_{\text{co,fast}}$ of the planet contribute to migration; co-orbiting planetesimals beyond this distance do not contribute. Integrating over this annulus, as in Equation (7), and using $r_{\text{H}} \propto m^{1/3}$, the attenuation factor scales

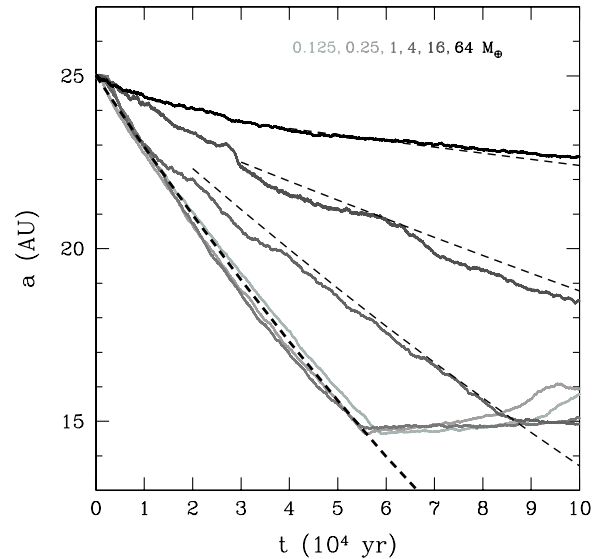


Figure 3. Migration of planets with different masses through a planetesimal disk. The disk is a sea of equal-mass particles, with $\Sigma = 1.2(a/25 \text{ AU})^{-1} \text{ g cm}^{-2}$, extending from 14.5 AU to 35.5 AU (e.g., Kirsh et al. 2009). Planetesimals have masses of 1/600th the mass of the planet and initial rms eccentricity of $1 e_{\text{H}}$. The three lowest mass planets with $m < m_{\text{fast}} \approx 3 M_{\oplus}$ undergo fast migration (heavy dashed curve; Equation (13)), until they “bounce” off the inner edge of the disk. More massive planets migrate more slowly (light dashed curves), at a rate that scales with m_{fast}/m .

as m_{fast}/m . For $m > m_{\text{fast}}$, migration rates scale inversely with the mass of the planet.³

Figure 3 illustrates several numerical simulations of fast migration for planets with a broad range of masses. Following Kirsh et al. (2009), each planet lies embedded in a power-law disk extending from 14.5 AU to 35.5 AU with $\Sigma = 1.2(a/25 \text{ AU})^{-1} \text{ g cm}^{-2}$. We represent the disk with particles that are each 1/600th of the mass of the planet. To speed up the onset of fast migration, the co-orbital zone ($\delta r \leq r_{\text{H}}$) is initially clear of particles. We also scale the rms planetesimal eccentricity to keep the same initial $e = r_{\text{H}}/a$ for each planet. The nearly identical migration tracks for masses below $m_{\text{fast}} \approx 3 M_{\oplus}$ illustrate fast migration at the theoretical rate indicated by the dashed curve. When the planet encounters the inner edge of the disk, the rates fall to zero (and sometimes reverse sign). More massive planets follow tracks that reflect the $1/m$ attenuation of the fast migration rate for $m > m_{\text{fast}}$.

Several aspects of protoplanetary disks conspire to set limits on the *minimum* planet mass for fast migration. In a gaseous disk, small planetesimals with $St < \alpha$ are entrained in the gas, where $St = r \rho_g \Omega / \rho c_s$ is the Stokes number, r and ρ are the radius and mass density of a planetesimal, ρ_g is the local gas density, and c_s is the sound speed (see Youdin & Lithwick 2007; Chiang & Youdin 2010; Ormel & Klahr 2010, and references therein). Fast migration requires that the Hill radius of the planet exceed the scale height, h_s , of the planetesimals. Following Youdin & Lithwick (2007), $h_s = h \min(1, \sqrt{\alpha/St})$, where h is the scale height of the gas and α is the disk viscosity parameter. Adopting a simple expression for the disk scale height, $h = h_0(a/1 \text{ AU})^{9/7}$ (e.g., Kenyon & Hartmann 1987; Chiang & Goldreich 1997) and requiring $h_s < r_{\text{H}}$ yields a simple expression for the minimum

³ Using a different approach, Ward (1991) notes that migration saturates when the planet cannot drift across the co-orbital zone in a synodic period (see also Paardekooper & Papaloizou 2009a). Our derivation yields the mass dependence directly.

mass for fast migration in a gaseous protoplanetary disk

$$m_{\text{fast,min}} \gtrsim 36 f_{\text{st}} \left(\frac{h_0}{0.033} \right)^3 \left(\frac{a}{1 \text{ AU}} \right)^{3/4} M_{\oplus} \quad (11)$$

where $f_{\text{st}} = \min(1, (\alpha/St)^{3/2})$. When $f_{\text{st}} = 1$, Equation (11) yields an approximate condition for fast (type III) migration through the gaseous disk (e.g., Equation (28)); see also Masset & Papaloizou 2003; D'Angelo et al. 2005; Crida et al. 2006; Peplinski et al. 2008a, 2008b). When most of the solid material is in much larger particles with $St \gg 1$, lower mass planets undergo fast migration through the planetesimals. For 1 km planetesimals with $St \sim 10^3$ and $\alpha = 10^{-2}$, $m_{\text{fast,min}} \approx 10^{-6} M_{\oplus}$ at 1 AU.

In a planetesimal disk, particle growth sets another limit on the minimum mass for fast migration. During oligarchic growth, leftover planetesimals have typical velocity dispersions, $v \approx \epsilon v_{\text{esc}}$, where v_{esc} is the escape velocity of the largest oligarch and $\epsilon \approx \Sigma_o/\Sigma_s$ is the ratio of the surface density in oligarchs to the surface density in planetesimals (e.g., Goldreich et al. 2004; Kenyon & Bromley 2008, 2010). The scale height of the planetesimals is then $h_s = v\Omega^{-1} \approx \epsilon v_{\text{esc}}\Omega^{-1}$, leading to a simple expression for the ratio of the scale height to the Hill radius in a disk surrounding a solar-type star

$$\frac{h_s}{r_{\text{H}}} \approx 20\rho^{1/6}\epsilon. \quad (12)$$

Thus, planets undergo fast migration through planetesimals only when they contain no more than $\sim 5\%$ ($\epsilon \lesssim 0.05$) of the mass in solid material.

2.1.3. Migration Rate Summary

Here, we summarize the migration rates calculated from Equation (7) for fast migration (with the reduction factor for large masses), and for a planet embedded in a disk that moves relatively slowly through small-angle scattering:

$$\frac{da_{\text{fast}}}{dt} = \pm 3.9 \frac{\pi a^2 \Sigma}{M} \left(\frac{X_{\text{co}}}{1.8} \right)^3 \min(1, m_{\text{fast}}/m) \frac{a}{T}, \quad (13)$$

$$\frac{da_{\text{emb}}}{dt} = -32(2-n) \frac{\pi a^2 \Sigma m}{3M^2} \frac{a^2}{\delta R^2} \frac{a}{T}, \quad (14)$$

$$= -\frac{8}{3}(2-n) \frac{\pi a^2 \Sigma}{M} \left(\frac{m}{3M} \right)^{1/3} \frac{r_{\text{xing}}^2}{\delta R^2} \frac{a}{T}, \quad (15)$$

where δR is the physical distance separating the planet and the edge(s) of the disk. The \pm sign for fast migration indicates it can be either inward or outward, at least for small-mass planets. In each case, we have kept only leading order terms in r_{H}/a and have assumed that the inner and outer edges of the disk are far, far away from the planet.

In a thorough analysis of the orbits of moonlets embedded in Saturn's ring system, Crida et al. (2010) derive $g(x)$ in the chaotic regime. Their Equation (39) for the migration rate has the same functional form as our Equation (15), including the $m^{1/3}$ dependence. Because we derive rates in the small-scattering limit, the numerical coefficient in Equation (15) is a few times smaller than the equivalent coefficient in the Crida et al. (2010) rate. Considering the differences in the two approaches, the agreement in the functional form and the magnitude of the migration rate is encouraging.

The migration timescale is $\tau \equiv a/|da/dt|$. For a planet embedded in a power-law disk (Equation (8)), the fast migration mode and slow, embedded migration yield

$$\tau_{\text{fast}}(\text{yr}) = 2.3 \times 10^4 \max(1, m/m_{\text{fast}}) \quad (16)$$

$$\tau_{\text{emb}}(\text{yr}) = 3.6 \times 10^6 \frac{(\delta R/a)^2}{0.035^2} \left(\frac{m}{M_{\oplus}} \right)^{-1} \quad (17)$$

$$= 3.6 \times 10^6 \frac{\delta R^2}{r_{\text{xing}}^2} \left(\frac{m}{M_{\oplus}} \right)^{-1/3} \quad (18)$$

for fiducial parameters of $M = 1 M_{\odot}$, $a = 1 \text{ AU}$, and $\Sigma_0 = 30 \text{ g cm}^{-2}$. For other situations, these timescales vary as

$$\tau \propto a^{n-1/2} \Sigma_0^{-1} M^b, \quad (19)$$

where $b = 1/2$ for fast migration with $m < m_{\text{fast}}$, $b = 3/2$ for embedded migration at fixed $\delta R/a$ (Equation (17)), and $b = 5/6$ for embedded migration at fixed dR/r_{xing} . The dependence on these parameters is more complicated for attenuated fast migration, with $m > m_{\text{fast}}$ (cf. Equation (10)).

Although fast migration is two orders of magnitude faster than the slow mode, embedded migration may sometimes dominate. In Equations (17) and (18), δR is the distance between the planet and the nearby edges of the disk. By construction, $\delta R > r_{\text{xing}}$. If the disk is dynamically warm, all interactions except for the small-angle scatterings are washed out. In a dynamically cold disk, a planet might make its own gap by scattering away all but the more distant material (e.g., Rafikov 2001). These two situations are similar to type I and type II migration in a gaseous disk (Section 3).

For many of these migration modes, the power-law variation of τ with a in Equation (19) yields an integrable expression for $a(t)$. In all modes of fast migration and embedded migration with a constant or slowly varying ratio $\delta R/a$ (e.g., Alexander & Armitage 2009), we can adopt $da/dt = Ca^{\gamma_1}$, where $\gamma_1 = 3/2 - n$, and derive a simple expression for the time variation of the semimajor axis

$$a(t) = \left[-\frac{Ct}{2\gamma_2-1} + a(0)^{1/\gamma_2} \right]^{\gamma_2}, \quad (20)$$

where $\gamma_2 = 2/(2n-1)$. Standard models for the minimum mass solar nebula (e.g., Weidenschilling 1977; Hayashi 1981) have $n = 3/2$; the semimajor axis of the orbit then contracts linearly with time. Radio observations of young stars are more consistent with $n = 1$ (e.g., Andrews & Williams 2007; Isella et al. 2009); a then contracts quadratically with time. Figure 4 compares our numerical simulations with the analytic results for $a(t)$.

To apply these results to more realistic disks with planets and planetesimals, we consider several examples derived from our planet formation simulations. We begin in Section 2.2 with disks stirred by growing protoplanets, continue in Section 2.3 with disks declining rapidly in mass, and conclude in Section 2.4 with disks containing many growing planets.

2.2. Stirred Disks

In the planetesimal theory, planets form by accreting smaller objects along their paths. When planetesimals are large ($r \gtrsim 0.1 \text{ km}$), growing planets gravitationally stir up the orbits of neighboring planetesimals (Artymowicz 1997; Kenyon &

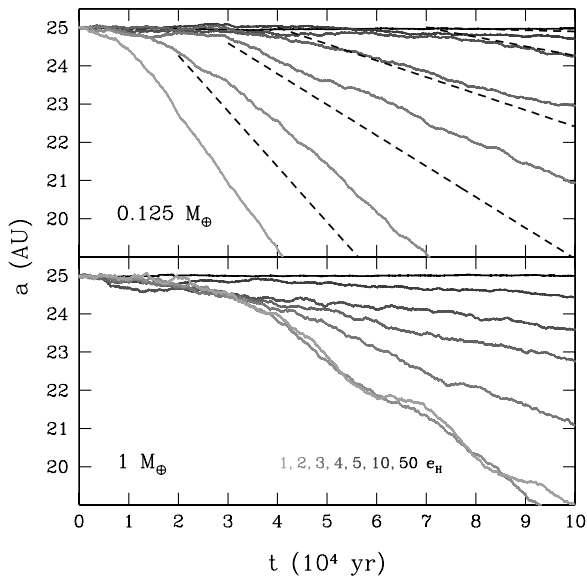


Figure 4. Planetary migration in disks with Σ as in Figure 3 and various values for the initial rms eccentricity. The lower left corner of each panel indicates the mass of the planet. In each panel, the initial e_H varies from 1 to 50 as indicated in the legend of the lower panel (lighter shades correspond to smaller initial eccentricity). The dashed curves in the upper panel show predicted rates from Equation (21).

Luu 1998; Kenyon & Bromley 2002). Thus, growing planets dynamically heat up the disk. In Hill units, with $e_H \equiv ea/r_H$, ensembles of growing planets rarely produce planetesimals with $e_H \lesssim 5$, where e is the orbital eccentricity of a planetesimal. During runaway growth, planets grow to masses of roughly 0.001–0.01 M_\oplus ; the rms eccentricities of planetesimals usually drop from $e_H \sim 100$ to $e_H \sim 5$. Throughout oligarchic growth, $e \propto \epsilon v_{\text{esc}}/v_K$, where v_{esc} is the escape velocity of the most massive planet, v_K is the local circular velocity, and ϵ is the ratio of the mass in oligarchs to the mass in planetesimals (e.g., Kenyon & Luu 1998; Goldreich et al. 2004; Kenyon & Bromley 2008). In Hill units, $e_H \propto \epsilon v_{\text{esc}}/r_H \propto \epsilon$. Thus, e_H grows slowly as oligarchs accrete more and more planetesimals, reaching $e_H \sim 100$ during the late stages of oligarchic growth and throughout chaotic growth (Kenyon & Bromley 2004, 2006, 2008, 2010). Inclinations are typically half of these values.⁴

In a hot disk, interactions between a planet and surrounding planetesimals weak, slowing the migration rate by a factor of (see Ida et al. 2000; Kirsh et al. 2009)

$$\frac{da}{dt} \gtrsim \left. \frac{da}{dt} \right|_{e_H=0} [1 + (e_H/3)^3]^{-1}. \quad (21)$$

To test this prediction, we repeat the calculations for Figure 3 and vary the rms value of the initial e_H for planetesimals from unity to 50. For larger values of initial e_H , migration is undetectable in a 10^5 yr time frame. For $e_H \approx 10$ –50, it is a challenge to prohibit particles from the co-orbital zone at the start of the simulation. To keep all calculations in this suite on the same footing, we allow planetesimals for all initial e_H to reside in the co-orbital zone. The fraction of particles in the co-orbital zone is small; most are not on horseshoe orbits. Still, the onset

⁴ In a disk where oligarchs grow from collisions with small planetesimals coupled to the gas, e and i are set through interactions with the gas instead of stirring by oligarchs (Section 2.1.2). When the gas produces $e > e_H$, migration slows as in Equation (21).

of the fast migration mode is somewhat slow compared to the results in Figure 3.

The results of these simulations (Figure 4) follow the trend expected from Equation (21). Planets embedded in a disk of low-eccentricity planetesimals migrate rapidly, at a rate that scales inversely with the mass of the planet (see also Figure 3). As we raise the initial e_H , the migration rate slows. For $e_H \approx 50$, the migration rate is negligible. As shown by the dashed lines in the upper panel of the figure, the reduction in the migration scales roughly as e_H^{-3} .

2.3. Eroded Disks

As an individual planet migrates through a disk annulus, it disrupts the disk (Ida et al. 2000; Kirsh et al. 2009). In fast migration, a planet tosses material into relatively eccentric orbits in random directions. This scattering process reduces the local surface density of planetesimals. If the planet moves fast enough to encounter only the unperturbed disk upstream from it, this disturbance has little adverse impact on the planet’s migration rate.

For more massive planets, slower migration may lead to a continuous loss of disk material. Planets migrate more slowly in less massive disks. To quantify this effect, we let the disk surface density within r_H of the planet vary as

$$\dot{\Sigma}(a, t) = -\frac{\epsilon}{T_{\text{syn}}} \Sigma(a, 0), \quad (22)$$

where t is the time since a planet reaches a narrow annulus of the disk at orbital distance a and ϵ describes the efficiency of a planet in scattering disk material. To derive the migration rate for a disk with this exponentially decaying surface density, we integrate Equation (22) over the time it takes the planet to migrate a distance r_H from Equation (7). Thus, we approximate the instantaneous surface density by a temporal and spatial average inside an active zone of width $O(r_H)$, where $\epsilon \sim r_H/a$ is an efficiency factor for clearing the zone of planetesimals. This approximation leads to a nonlinear equation where the average value of Σ depends on the migration rate. Solving this equation leads to a new migration rate

$$\frac{da}{dt} \approx \frac{3\epsilon r_H^2}{2aT} \left[\ln \left(1 - \frac{3\epsilon r_H^2}{2a\dot{a}_0 T} \right) \right]^{-1}, \quad (23)$$

where \dot{a}_0 is the theoretical migration rate of the planet without any time variation in the disk surface density. The sensitivity of this model to the exact form of ϵ is fairly weak.

When the argument of the logarithm in Equation (23) is zero, the migration rate vanishes. Thus, this expression implies a high-mass cutoff, m_{erode} , where more massive planets cannot migrate through the disk. From Equation (13), this limit is

$$m_{\text{erode}} \sim \sqrt{8\pi a^2 \Sigma m_{\text{fast}}} \quad (24)$$

$$\sim 0.8 \left(\frac{a}{1 \text{ AU}} \right)^{7/4-n/2} M_\oplus. \quad (25)$$

If disk erosion is an important process, it begins when a planet reaches roughly an Earth mass at 1 AU and over 40 M_\oplus at 25 AU. Removal of disk material by scattering is at least enhanced, if not entirely enabled, by secondary scattering from nearby planets. Migration, in principle, can be virtually halted for higher mass planets if they have neighbors that prevent the return of scattered planetesimals.

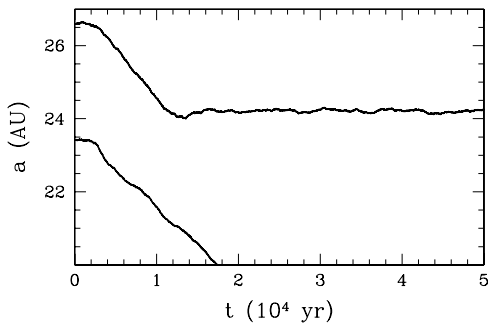


Figure 5. Disrupted migration of a planet as a result of stirring by its neighbor. The planetesimal disk has initial conditions as in Figure 3. Two $0.5 M_{\oplus}$ planets have initial separation of $16 r_H$. Each begins fast migration. The inward motion of the outer planet stops when it encounters the wake of excited planetesimals left behind by the inner planet.

2.4. Multiple Planets in a Disk

In the coagulation paradigm, planets grow hierarchically from smaller planetesimals. As they grow, planets almost always have neighbors of comparable mass. During runaway and oligarchic growth, a few large objects try to accrete all of the mass in an annulus. Once these oligarchs contain roughly half of the total mass, they begin to interact chaotically (Goldreich et al. 2004; Kenyon & Bromley 2006). During chaotic growth, planets scatter planetesimals to large e_H and grow by large collisions with other planets (Kenyon & Bromley 2006). Once chaotic growth begins, smooth migration through a sea of planetesimals is impossible. Thus, we consider migration in a disk of growing oligarchs which contain less than half of the mass in solid material.

Planets affect the migration of a neighboring planet in two ways. As a planet migrates through a disk, it stirs up the planetesimals along its orbit. After migrating past these excited planetesimals, the planet leaves behind a wake of planetesimals with large e_H (see also Edgar & Artymowicz 2004; Kirsh et al. 2009). This wake is a barrier that prevents other planets from migrating inward from larger a . For a planet migrating through a disk with initial $e_H \approx 1$, planetesimals left behind have typical $e_H \gtrsim 3-5$. From Equation (21), planets encountering stirred up planetesimals have factor of 2–6 times smaller migration rates. In addition, planets migrating into a wake require longer periods to clear their co-orbital zones of dynamically “hot” planetesimals. As a result of these factors, migration ceases.

Figure 5 illustrates this phenomenon. Two planets migrate inward in the fast migration mode; the migration of the outer planet stops abruptly when it encounters the wake of planetesimals already stirred up by its partner.

Migrating planets can also deflect planetesimals that chaotically scatter from a neighboring planet. When a planet deflects planetesimals from its neighbor, it prevents the planetesimals from returning to the neighbor. The loss of these encounters prevents the neighbor from migrating toward the planet. Thus, the two planets recoil from the material that is passed between them (see also Malhotra 1993; Hahn & Malhotra 1999).

To demonstrate this process, we simulate the migration of a Saturn-mass planet at 10 AU embedded in a massive disk ($400 M_{\oplus}$ between 6 AU and 20 AU, with a power-law surface density distribution and $n = 1$; see Levison et al. 2007). We then vary the mass of a second planet at 5 AU. As the mass of the inner planet falls from a jovian mass to $30 M_{\oplus}$, the sense of migration of the outer planet changes from outward (Figure 6; black curves) to inward (blue curve). Until it encounters scattered

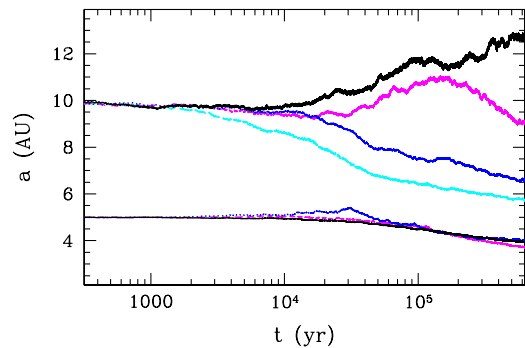


Figure 6. Migration of a Saturn-mass planet in a planetesimal disk with initial conditions as in Figure 9 of Levison et al. (2007). The disk extends from 6 AU to 20 AU and has a mass equal to the combined mass of Jupiter and Saturn. The Saturn-mass planet begins at 10 AU. The inner planet starts at 5 AU and has the mass of Jupiter (black), Saturn (magenta), and $30 M_{\oplus}$ (blue). The cyan curve shows the outer planet migrating through the disk in the absence of any other planet.

(A color version of this figure is available in the online journal.)

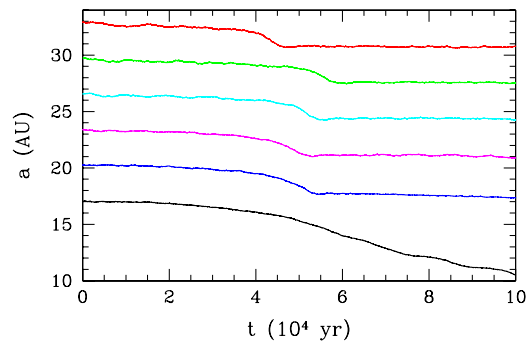


Figure 7. Migration of multiple planets in a planetesimal disk with initial conditions as in Figure 3 except that the inner edge of the disk is at 5 AU. Six $0.5 M_{\oplus}$ planets separated by $16 r_H$ migrate inward until they encounter the wakes of their inner neighbor. Once the innermost planet reaches ~ 10 AU, its mass exceeds m_{fast} . Because $m_{\text{fast}} \propto a^{3/2}$, its migration rate then slows dramatically.

(A color version of this figure is available in the online journal.)

planetesimals from the outer planet, the inner planet slowly migrates inward at the “adjacent” rate from Equation (9). Despite its small Hill radius ($r_H = 0.155$ AU), the $30 M_{\oplus}$ inner planet has a considerable impact on the migration rate of a much more massive outer planet 5 AU away. Migration is remarkably fragile.

To conclude this section, we consider migration in a multi-planet system. In our simulations of planet formation (e.g., Kenyon & Bromley 2006; Bromley & Kenyon 2011), planets with masses of $0.1-1 M_{\oplus}$ are often separated by 10–20 mutual Hill radii. To investigate migration in an idealized version of these calculations, we simulate the evolution of six $0.5 M_{\oplus}$ planets in a disk of planetesimals extending from 7–35.5 AU. As in the calculations for Figure 3, the planetesimals have an initial surface density distribution $\Sigma = 1.2(a/25 \text{ AU})^{-1} \text{ g cm}^{-2}$. Unlike the calculations in Figure 3, co-orbital zones are initially filled with planetesimals.

Figure 7 summarizes the main results of these simulations. In a multi-planet system, long-term migration rates are small. Initially, each planet clears its co-orbital zone of material in $3-6 \times 10^4$ yr. Fast migration commences. Eventually, each planet encounters the ensemble of stirred up planetesimals left behind by its inward neighbor. Migration stops. In these examples, migration of the innermost planet ceases when it reaches the

inner edge of the disk. In disks with small inner radii, migration of the outer planets ceases well before the inner planet reaches the inner edge of the disk.

2.5. Migration and Planet Formation

To place these results in the context of formation scenarios, we consider the growth and migration of planets in the planetesimal theory. In this picture, planetesimals ranging in size from ~ 0.1 km to ~ 100 km condense out of the gaseous disk. Planetesimals collide and merge into larger and larger objects. After short periods of orderly and runaway growth, the largest objects enter oligarchic growth, where they continue to accrete and to stir up leftover planetesimals. During this phase, dynamical friction between planetesimals and oligarchs dominates dynamical interactions among oligarchs. Thus, oligarchs remain fairly isolated from one another. Once oligarchs contain roughly half of the mass in solid material, their mutual dynamical interactions dominate dynamical friction with planetesimals. Oligarchy ends. Chaotic growth, where oligarchs grow by giant impacts and continued accretion of small planetesimals, begins (Goldreich et al. 2004; Kenyon & Bromley 2006)

During the transition from oligarchic to chaotic growth, the “isolation mass” sets the mass of the largest oligarchs (Lissauer 1987; Kokubo & Ida 1998; Goldreich et al. 2004). By definition, isolated objects have small dynamical interactions; thus, their typical separations are $\sim Br_H$ with $B \approx 7\text{--}10$ (Lissauer 1987; Kokubo & Ida 1998, 2000, 2002). When an object contains all of the mass in an annulus of width Br_H , it reaches the isolation mass. With $m_{\text{iso}} = 2\pi a \Sigma Br_H$ and $\Sigma = \Sigma_0 a^{-n}$, $m_{\text{iso}} = (2\pi B \Sigma_0)^{3/2} (3M)^{-1/2} a^{3-3n/2}$. If we adopt a disk with $n = 1$, $\Sigma_0 = 10 \text{ g cm}^{-2}$, and $B = 7$, isolated objects have separations of $2r_{\text{xing}} = Br_H$ and lie well outside the co-orbital zones of their nearest neighbors. The isolation mass is then⁵

$$m_{\text{iso}} = 0.07 \left(\frac{\Sigma_0}{10 \text{ g cm}^{-2}} \right)^{3/2} \left(\frac{a}{1 \text{ AU}} \right)^{3/2} \left(\frac{1 M_{\odot}}{M} \right)^{1/2} M_{\oplus}. \quad (26)$$

For each oligarch, the ratio of m_{iso} to m_{fast} (Equation (10)) sets the importance, the mode, and the timing of migration through a sea of planetesimals. Low-mass oligarchs with $m_{\text{oli}} < m_{\text{iso}}$ can migrate, but they cannot migrate freely. The typical radial spacing of low-mass oligarchs is $r_{\text{oli}} \approx 7(m_{\text{oli}}/m_{\text{iso}})^{2/3} r_H$. With $r_{\text{oli}} \ll 7r_H$, an oligarch migrates only a few r_H before it encounters the wakes of other oligarchs. Migration then ceases. Once massive oligarchs have $m \gtrsim m_{\text{iso}}$, they are free to migrate. However, massive oligarchs also interact chaotically. At 1–10 AU, the timescale for chaotic growth is shorter (longer) than the timescale for slow (fast) migration. When $m_{\text{iso}} < m_{\text{fast}}$, migration is important during chaotic growth. Otherwise, growing oligarchs do not migrate through a sea of planetesimals.

This analysis suggests that migration through an ensemble of planetesimals is rarely important within planet-forming disks. From our definitions of m_{iso} and m_{fast} (Equation (10)), the ratio $m_{\text{iso}}/m_{\text{fast}} = 3B^2/4 \approx 37$. Although growing oligarchs migrate in the fast mode, they can never migrate very far before they encounter the wake of another migrating oligarch. Migration then ceases (Figures 5 and 7).

There are several plausible exceptions to this conclusion. If collisional damping or gas drag reduce the e and i of stirred up planetesimals in the wake of a migrating planet, then another planet can migrate through the wake. When the wake consists of large planetesimals with $r \gtrsim 0.1$ km, however, collisional damping and gas drag are ineffective. Dynamical friction and viscous stirring by large planetesimals and small oligarchs keep particles at large e and i (e.g., Kenyon & Luu 1998; Goldreich et al. 2004). Thus, oligarchs cannot migrate freely through a disk of large planetesimals. For smaller particles, damping may reduce e and i on timescales comparable to the migration timescale (e.g., Kenyon & Bromley 2001). Because damping and migration occur on similar timescales, closely spaced oligarchs probably encounter wakes before damping can smooth them out. Widely spaced oligarchs suffer chaotic growth, which keeps planetesimals stirred up despite damping. Thus, we conclude that damping does not allow migration in a planetesimal disk.

Scattering may also lead to effective migration (Levison et al. 2007; Raymond et al. 2009a, 2010). During chaotic growth, massive planets scatter lower mass planets farther out in the disk (e.g., Marzari & Weidenschilling 2002; Veras et al. 2009; Raymond et al. 2010; Bromley & Kenyon 2011; Chatterjee et al. 2010). At large a , oligarchs form slowly (e.g., Kenyon & Bromley 2008, 2010). Thus, planets formed at small a and scattered to large a may end up in a calm disk composed of planetesimals with small e_H . Without other oligarchs to impede them, these scattered planets can then migrate freely through the outer disk.

Once chaotic growth ends, any leftover planetesimals can support inward or outward migration. For leftovers with large e and i , migration rates are slow. However, outwardly migrating planets may reach planetesimals with much lower e and i , enhancing migration rates. Several dynamical models for the origin of the solar system rely on migration through a leftover planetesimal disk (e.g., Hahn & Malhotra 1999; Tsiganis et al. 2005). As planets migrate outward, they may capture objects in orbital resonances. This process may yield some dynamical classes of trans-Neptunian objects (e.g., Morbidelli et al. 2008) and dense clumps of material in debris disks (e.g., Wyatt 2003; Wyatt et al. 2005; Martin et al. 2007; Crida et al. 2009).

To conclude this section, Figure 8 compares the variation of m_{iso} and m_{fast} with semimajor axis for a plausible disk model. We adopt a disk with $\Sigma = \Sigma_0 a^{-1}$ and $\Sigma_0 = 10 \text{ g cm}^{-2}$ at 1 AU. Here, we assume a factor of three jump in the surface density of solid material at the snow line, $a_{\text{snow}} = 3 \text{ AU}$. We ignore the likely variation in the position of the snow line with time (Kennedy & Kenyon 2008). In this disk model, m_{fast} ranges from $0.005 M_{\oplus}$ at 1 AU to $\sim 1 M_{\oplus}$ at 10 AU; m_{iso} grows from $0.07 M_{\oplus}$ at 1 AU to $10 M_{\oplus}$ at 10 AU. Based on our simulations, low-mass oligarchs with $m < m_{\text{iso}}$ are too closely packed to migrate. Prior to chaotic growth, planetesimals can grow to reasonably massive oligarchs. With $m_{\text{erode}} > m_{\text{iso}}$ at all a , disk erosion is also unimportant. Once masses reach m_{iso} , chaotic growth without migration leads to terrestrial-mass planets at 1 AU (Raymond et al. 2005; Kenyon & Bromley 2006; Raymond et al. 2009b) and Jupiter-mass planets at 3–30 AU (Goldreich et al. 2004; Bromley & Kenyon 2011).

3. RELATIONSHIP TO MIGRATION IN GASEOUS DISKS

To explore whether our results on migration are general, we now consider some analogies between migration in gaseous and planetesimal disks. As motivation, numerical simulations

⁵ Our definition is appropriate for the onset of chaotic growth, when $e_H > 1$; when $e_H < 1$, the alternative of Goldreich et al. (2004) provides a better measure of the masses of isolated objects.

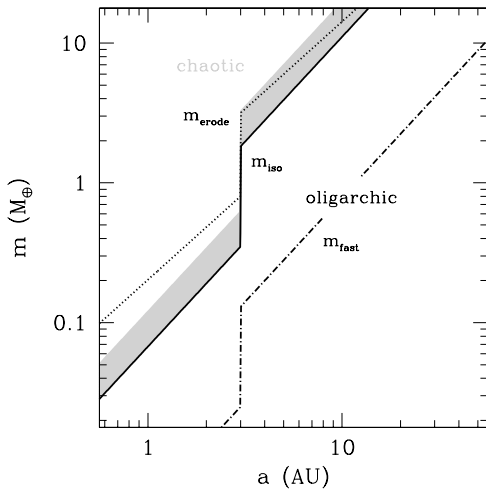


Figure 8. Growth and migration modes in a planetesimal disk. The heavy solid curve and the shaded region indicate the variation of the isolation mass (m_{iso}) with semimajor axis; planets with $m < m_{\text{iso}}$ ($m > m_{\text{iso}}$) undergo oligarchic (chaotic) growth. The dot-dashed curve indicates the variation of m_{fast} with a ; planets with $m < m_{\text{fast}}$ ($m > m_{\text{fast}}$) undergo fast (slow) migration. Until planets reach m_{iso} , they are tightly packed and unable to migrate large distances through the disk. Once they have $m > m_{\text{iso}}$, they are free to migrate in the slow mode. As planets grow larger than m_{iso} , their migration may be slowed by disk erosion, as indicated by the dotted line (m_{erode}).

demonstrate that systems of many oligarchs are likely outcomes of runaway growth in a planetesimal disk. Although there are several elegant approaches to the migration of single planets in a gaseous disk (see Papaloizou et al. 2007, and references therein), generalizing these approaches to systems of 20–30 (or more) planets with masses comparable to or less than the isolation mass is challenging (see Cresswell & Nelson 2006, 2008). Here, we try to see whether we can apply results for planetesimal disks to gaseous disks.

In the limit of zero viscosity, equal mass gaseous and particle disks provide an identical torque on an embedded planet (Goldreich & Tremaine 1980). In both types of disk, local variations in density generate the torque. In a particle disk, scattering sets the density structure. In a continuous medium, a balance between gravity, pressure, and viscous forces sets the density structure. As the viscosity of the medium increases,

this structure damps out. In this heuristic picture, planetesimals generate migration efficiently; a very viscous medium cannot generate migration. However, the large mass of a gaseous disk gives it an overwhelming advantage over a planetesimal disk. For a solar metallicity system, the gaseous disk is roughly 100 times more massive than the disk of solids.

As predicted by Goldreich & Tremaine (1980), our numerical simulations produce coherent wakes from orbital resonances close to embedded planets. In planetesimal disks (Figure 9), an embedded planet scatters planetesimals out of the co-orbital zone into disk regions several r_H away from the planet. The region of horseshoe orbits is initially filled (as in Figure 9, left panel); continued scattering removes planetesimals from the co-orbital zone (as in Figure 9, right panel). In both panels, a bridge of enhanced planetesimal density connects the high density rings of planetesimals lying $\pm 4\text{--}5 r_H$ away from the orbit of the planet. Because the 2:1 resonance lies outside the disk, the strongest density enhancements lie at the 3:2, 4:3, and 5:4 resonances.

To illustrate the time evolution of these structures, the online version of this paper contains an animation of a planet migrating from 25 AU to 15 AU in $\sim 8 \times 10^4$ yr. Throughout the animation, the planet scatters planetesimals out of its orbit into various resonances. Figure 10 shows a snapshot from the animation. At this point of the evolution, the planet has migrated from 25 AU to ~ 20 AU. At 25 AU, the original orbit of the planet is nearly devoid of planetesimals. Just outside this orbit, the density of planetesimals is somewhat higher than the initial density. Between 20 AU and 25 AU, the planet has left behind a sea of stirred up planetesimals, with several density enhancements at orbital resonances. At 20 AU, the planet has evacuated planetesimals downstream from its orbit. Upstream, planetesimals remain in horseshoe orbits.

The structures in planetesimal disks are similar to those produced in simulations of gaseous disks (e.g., Bate et al. 2003; D’Angelo et al. 2003; Klahr & Kley 2006; Paardekooper & Mellema 2006a). In all of the simulations of planets within gaseous disks, torques between the planet and the disk create local enhancements in the gas density at orbital resonances as well as the bridge of material from the planet to the bright rings. For disks with similar surface density distributions and planets with similar masses, the derived range of the

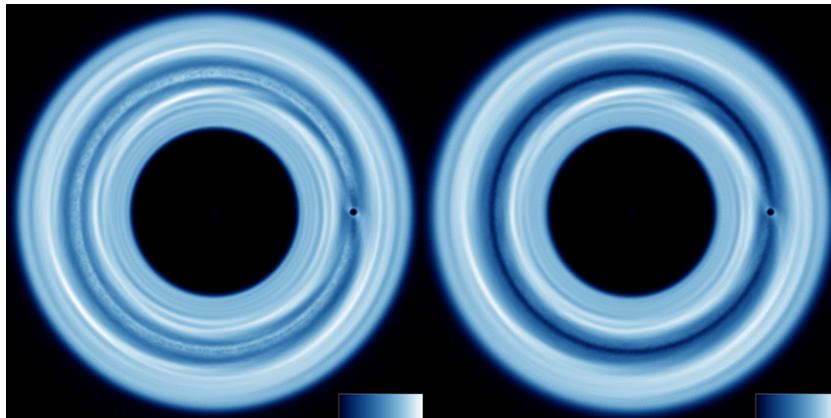


Figure 9. Density wakes in planetesimal disks with an embedded planet. Both images are in a frame rotating with the planet, which has a mass of $16 M_{\oplus}$ and a semimajor axis of 25 AU. In the left panel, the corotation zone contains planetesimals; in the right panel, the corotation zone is empty. From the inner edge of the disk at ~ 15 AU to the outer edge at ~ 35 AU, the images show the local planetesimal density—averaged over 1 kyr—relative to the initial surface density, $\Sigma(a) = 30 \text{ g cm}^{-2}(a/1 \text{ AU})$. In the lower right corner of each image, the scale shows the linear map of density to color. The full range of the color map is a factor of two in the local mean density.

(A color version of this figure is available in the online journal.)

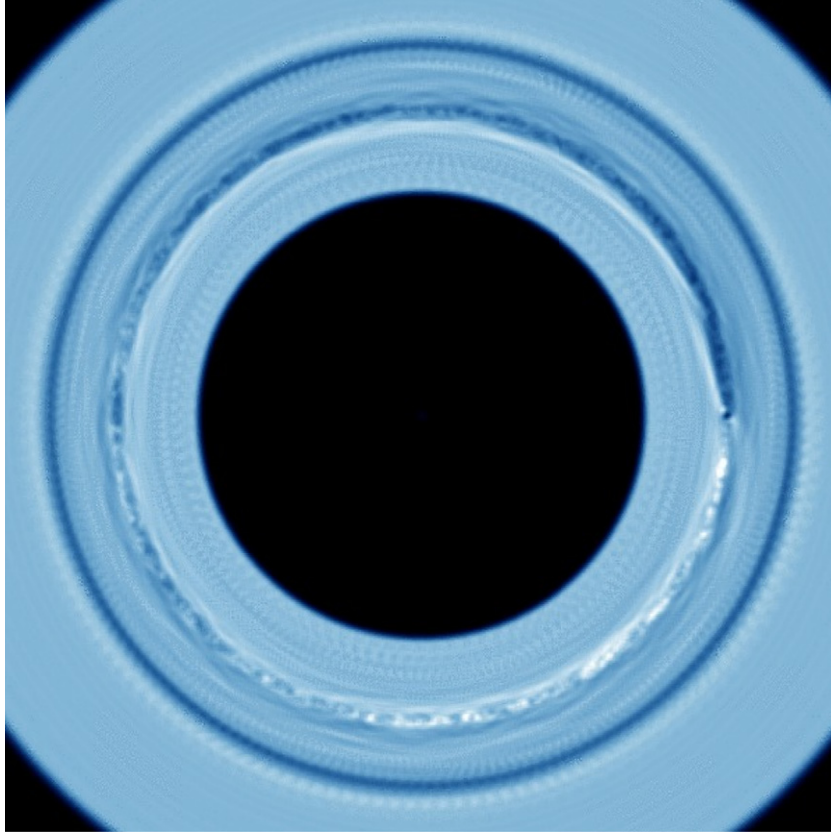


Figure 10. As in Figure 9 for a planet experiencing fast migration. This image is a snapshot from a simulation of a $1 M_{\oplus}$ planet, available in the online version of the journal. The simulation shows density structures after the planet has moved several AU inward from its initial orbital distance at 25 AU. When the planet is in fast migration mode, the upstream corotation zone is filled; the downstream region is relatively empty.

(An animation and a color version of this figure are available in the online journal.)

density enhancements are also similar (see, for example, Ward 1997; D’Angelo & Lubow 2008). Because gaseous disks have some pressure support, co-orbital gas lies a small distance, $\delta r_{\text{co}} \approx 0.002\text{--}0.004a$, inside the orbit of a planet (e.g., Tanaka et al. 2002). When co-orbital gas lies inside the Hill sphere of the planet ($m \gtrsim 0.03 M_{\oplus}$), we expect co-orbital gas and planetesimals with similar surface density to exert similar torques on a nearby planet. Thus, gaseous and planetesimal disks should produce comparable migration rates for planets with $m \gtrsim m_{\text{iso}}$.

3.1. Migration Timescales

To generalize our migration results to a gaseous disk, we consider the vertical scale height of the disk h as a smoothing length, which sets the minimum size of density features in the disk. In type I migration, this assumption limits the scale and the location of the density wakes that form through interaction with a relatively small planet. The largest wakes lie at a distance $\delta R \sim h \gg r_{\text{H}}$. Thus, we can use results for small-angle scattering. For gaseous disks, the standard type I rate for an isothermal disk from Tanaka et al. (2002) is

$$\frac{da_1}{dt} = -(2.7 + 1.1n) \frac{2\pi a^2 \Sigma_g m a^2}{M^2 h^2 T}, \quad (27)$$

where Σ_g is the surface density of the gaseous disk at a . Setting $\delta R \sim h$ and assuming the planetesimals and the gas have the same surface density at the position of the planet, the ratio of the rate from Equation (14) to this rate is $\xi_I = 16(2 - n)/3(2.7 + 1.1n)$. Additional features in the Tanaka

et al. (2002) derivation, including three-dimensional effects and corotation resonances, produce the different dependence on the surface-density power-law index n . For $n = 0.5\text{--}1.5$, $\xi_I \approx 2\text{--}0.5$; thus, the rates differ by a small numerical factor.⁶ Clearly, small-angle-scattering migration in a planetesimal disk and type I migration in a gaseous disk share general properties.

Type II migration occurs when a relatively massive planet creates a gap in a gaseous disk and locks into the disk’s viscous flow as a result of a build-up of material at the gap’s edges. Gravitational torques exerted on the planet by the disk produce inward migration. Thus, the planet responds to the instantaneous density perturbations within the disk. These perturbations are strongest at the gap edges, which are several r_{H} away from the planet. The condition for gap opening is an elegant inequality between m , h , and the disk viscosity parameter α (Crida et al. 2006):

$$\frac{3}{4} \frac{h}{r_{\text{H}}} + 50\alpha \frac{M}{m} \left(\frac{h}{a}\right)^2 \lesssim 1, \quad (28)$$

where $\alpha = \nu/h^2\Omega$, ν is the disk viscosity, and Ω is the angular velocity (e.g., Pringle 1981). This constraint has a simple physical interpretation. When the viscosity is small ($\alpha \rightarrow 0$), the first term dominates; planets with Hill radii comparable to the local disk scale height open a gap (see also Ward 1997; Lin & Papaloizou 1986, 1993, and references therein). As the viscosity grows ($\alpha \rightarrow 1$), the second term dominates; planets

⁶ Using the more recent type I rate from D’Angelo & Lubow (2010) yields similar results.

with tidal forces large enough to overcome viscous transport open a gap (e.g., Ward 1997; Bryden et al. 1999).

From the condition for gap opening in the low viscosity limit and the Tanaka et al. (2002) type I migration rate, Papaloizou et al. (2007) derive a simple estimate for the maximum type II rate. For planets with $m \approx 30\text{--}1000 M_{\oplus}$, their simple estimate agrees with rates derived from detailed numerical simulations (see Figure 3 of Papaloizou et al. 2007). Adopting $\delta R \approx r_H$ in the embedded migration timescale from Equation (18) and assuming the same Σ , we derive a ratio of rates $\xi_{II, \alpha=0} = 32(2-n)/3(5.4+2.2n) \approx 2.5\text{--}0.6$ for $n = 0.5\text{--}1.5$. Thus, both approaches yield the same scaling with r_H and magnitudes consistent to a factor of 2–3. In this limit, irradiation from the central star sets the scale height of the gas (e.g., Kenyon & Hartmann 1987; Chiang & Goldreich 1997). Once this scale is set, the mass of the planet establishes the region of the disk that interacts most strongly with the planet. In the zero viscosity limit, planetesimals and gas respond to the gravity of the planet on the Hill scale, leading to similar timescales.

In the large viscosity limit, our analogy between planetesimal and gaseous disks breaks down. Large viscosity enables a gaseous disk to transport mass inward and angular momentum outward. Viscous transport modifies the universal trajectory function $g(x)$. Identifying $g(x)$ for viscous transport is beyond the scope of this paper; however, we speculate that substituting proper expressions for $g(x)$ and the size of the gap in Equation (7) would yield a migration rate reasonably close to published type II rates, $da/dt \approx \alpha(h/a)^2 a \Omega$, where Ω is the angular velocity of the planet at semimajor axis a . Successfully applying our approach in the large α limit would link the theories of migration in gaseous and planetesimal disks.

Type III migration is completely analogous to the fast migration mode in planetesimal disks (Masset & Papaloizou 2003; see also Equation (11)). Because it regulates how efficiently material is transported across a planet’s orbital position, viscosity complicates precise comparisons between gaseous and particle disks. However, viscosity generally makes migration in gaseous disks less efficient per unit disk mass than in planetesimal disks (Ida & Lin 2008). As a result, planets with masses much less than the mass of Saturn are “safe” from type III migration through the gaseous disk (e.g., Masset & Papaloizou 2003; D’Angelo et al. 2005; Pepliński et al. 2008a, 2008b).

3.2. Migration with Multiple Planets

In a gaseous disk, there are three sources of torque on an embedded planet. Torque from an inner spiral density wave and material in the corotation zone produces a net outward migration. Material in an outer spiral density wave causes a net inward migration. As the planet migrates inward, viscous torques smooth out density perturbations behind the planet. Smoothing occurs on a local viscous timescale, which is comparable to the migration rate.

In a multiple planet system, each planet produces a pair of spiral density waves. Thus, each planet feels a torque from the spiral density waves of all planets and the gas in its corotation zone. When planets are widely separated, distant spiral density waves contribute little to the torque. Widely spaced planets migrate freely. When planets are tightly packed, many spiral waves contribute to the torque. In linear theory (e.g., Tanaka et al. 2002), multiple torques superpose and add to the migration. However, this approach does not address the response of the gaseous disk to the time-variable potential of a collection of closely packed planets. The gravitational potential of the planets

varies on timescales shorter than the viscous timescale, which should wash out spiral density waves and reduce migration rates.

Recent analyses show that the thermodynamics of the disk is an important factor in setting the direction and rate of type I migration (e.g., Paardekooper & Papaloizou 2008; Paardekooper et al. 2010, 2011). In these nonlinear calculations, migration of a single planet depends on the vertical temperature structure and the relative strength of torques from the corotation zone and the Lindblad resonances. In a multiple planet system, each corotation zone generally lies within a few Hill radii of a single planet; thus, closely packed planets may not change the torque from the corotation zone. Because Lindblad resonances lie many Hill radii away from a planet, they are easily perturbed by an ensemble of closely packed planets which change the density and temperature structure on timescales shorter than the viscous timescale. Because the disk responds relatively slowly to motions of the oligarchs, spiral density waves are probably much weaker in a system with many oligarchs than in a system with a few oligarchs. Weaker density waves produce smaller migration rates. By analogy with our simulations of planetesimal disks, we propose that tightly packed planets do not migrate.

To place quantitative constraints on these limits, we compare the locations of the resonances that drive migration to the radial spacing of planets. For type I migration, the gaseous disk produces the strongest torques at the inner and outer Lindblad resonances, which lie at orbital distances $\delta a_{LR} \approx \pm 2h/3$ from the migrating planet (e.g., Papaloizou et al. 2007). For two planets separated by $r \approx \pm 4h/3$, their Lindblad resonances overlap. This tight spacing may preclude the elegant spiral density waves necessary for type I migration. Planets separated by $r_{\min} \approx 2h$ have isolated Lindblad resonances and can migrate freely. With $h \approx h_0 (a/1 \text{ AU})^{9/7} \text{ AU}$ (Chiang & Goldreich 1997), this constraint becomes $r_{\min} \approx 0.06 (a/1 \text{ AU})^{9/7} \text{ AU}$ for $h_0 = 0.03 \text{ AU}$. To convert to Hill units, planets with $m \approx M_{\oplus}$ have $r_H \approx 0.01a$. Thus, our constraint is

$$r_{\min} \approx 6r_H \left(\frac{M_{\oplus}}{m} \right)^{1/3} \left(\frac{a}{1 \text{ AU}} \right)^{2/7}. \quad (29)$$

Numerical simulations do not yet address constraints on the ability of closely packed planets to undergo type I or type III migration. Cresswell & Nelson (2006, 2008) consider ensembles of Earth-mass or larger planets ($m \gtrsim m_{\text{iso}}$) spaced by roughly 5–7 r_H . In their simulations, type I migration is briefly interrupted by rapid, chaotic interactions among the planets. Once the planets have merged or scattered, type I migration continues. Calculations for systems of lower mass planets with $m \lesssim m_{\text{iso}}$ do not exist. For now, we assume that ensembles of lower mass planets with typical separations smaller than r_{\min} do not migrate.

3.3. Migration and Planet Formation

To establish some constraints on type I migration through a gaseous disk containing an ensemble of growing planetesimals, we generalize our discussion of isolated oligarchs from Section 2.5. As planetesimals experience runaway, oligarchic, and chaotic growth, the gaseous disk evolves with time. In addition to viscous evolution, photoevaporation and gas giant planet formation remove mass from the disk (Alexander & Armitage 2009). Observations of young stars suggest typical disk lifetimes of 1–3 Myr (Haisch et al. 2001; Currie et al. 2009; Kennedy & Kenyon 2009; Mamajek 2009; Williams & Cieza 2011). Thus, migration through the gaseous disk ceases after 1–3 Myr.

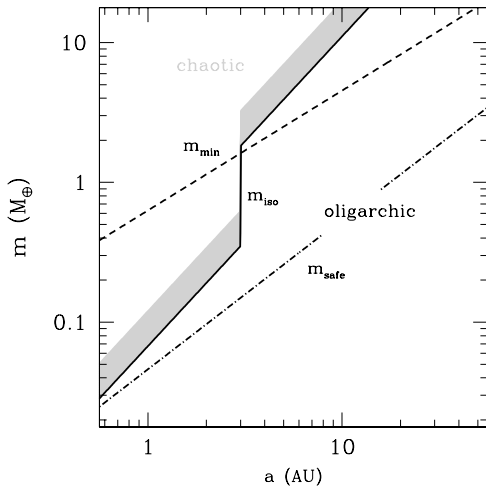


Figure 11. As in Figure 8 for a gaseous disk. Curves for isolation mass are also from Figure 8. Planets with $m < m_{\text{safe}}$ (dot-dashed line) migrate on timescales longer than the lifetime of the gaseous disk. Before they migrate significantly, the gas disperses. Planets with $m < m_{\text{min}}$ (dashed line) are packed too closely to migrate through the gaseous disk. Terrestrial planets likely undergo chaotic growth before they are able to migrate. The cores of gas giant planets start to migrate as they begin chaotic growth.

The lifetime of the gaseous disk places a rough lower limit on the masses of planets subject to type I migration. For the linear calculations of Tanaka et al. (2002), the timescale for type I migration is $\tau \propto m^{-1}$. Thus, lower mass planets migrate more slowly. Setting the timescale in Equation (9) of Papaloizou et al. (2007) to 3 Myr, we can derive an expression for the masses of planets that are safe from type I migration

$$m_{\text{safe}} \approx 0.046 \left(\frac{h/h_0}{0.03} \right)^2 \left(\frac{a}{1 \text{ AU}} \right)^{n+1/14} \quad (30)$$

$$\times \left(\frac{\Sigma_0}{1700 \text{ g cm}^{-2}} \right)^{-1} \left(\frac{M}{1 M_\odot} \right)^{3/2} M_\oplus, \quad (31)$$

where we assume a gaseous disk with $\Sigma = \Sigma_0 a^{-n}$. Planets with $m < m_{\text{safe}}$ migrate on timescales longer than the typical disk lifetime. Figure 11 compares the variation of m_{safe} and m_{iso} with semimajor axis. For all a , $m_{\text{iso}} \gg m_{\text{safe}}$. Low-mass oligarchs have long migration timescales; isolated objects are not safe from type I migration.

Despite their lack of safety, many isolated oligarchs are packed too tightly together to migrate. To draw this conclusion, we derive the masses of objects with $r_{\text{min}} = 7 r_{\text{H}}$, the typical separations of oligarchs at the onset of chaotic growth. Defining m_{min} as the mass where $r_{\text{min}} = 7 r_{\text{H}}$

$$m_{\text{min}} \approx 0.63 \left(\frac{a}{1 \text{ AU}} \right)^{6/7} M_\oplus. \quad (32)$$

In our picture, oligarchs with $m < m_{\text{min}}$ are packed too tightly to undergo type I migration. For $a \lesssim 5 \text{ AU}$, $m_{\text{min}} \gtrsim m_{\text{iso}}$; isolated oligarchs have overlapping Lindblad resonances and are packed too closely to migrate. At larger a , $m_{\text{min}} \lesssim m_{\text{iso}}$; oligarchs do not have overlapping resonances and can migrate.

This result leads to an important conclusion for terrestrial planet formation. If the overlapping Lindblad resonances of tightly packed oligarchs at 1 AU do not generate type I migration, chaotic growth produces Earth-mass or larger planets on

timescales of $\sim 10 \text{ Myr}$. In our simulations (e.g., Kenyon & Bromley 2006), it takes $\sim 3 \times 10^4 \text{ yr}$ ($\sim 10^5 \text{ yr}$) to produce 5–10 (~ 15) oligarchs with $m \sim 0.002\text{--}0.004 M_\oplus$ at 0.85–1.15 AU. These oligarchs are safe from type I migration through the gas (Figure 11), but their low masses allow fast migration through the sea of leftover planetesimals. However, growing oligarchs stir planetesimals to $e_{\text{H}} \gtrsim 5$. After migrating $\sim 0.02\text{--}0.03 \text{ AU}$, each oligarch encounters planetesimals stirred up by its inner neighbor. Relative to the standard fast migration rate, we estimate a factor of 10–100 reduction in the migration rate for each oligarch in our 2006 simulations. On the (reduced) migration timescale of $\gtrsim 10^6 \text{ yr}$, each oligarch in our simulations grows by more than an order of magnitude and begins to interact chaotically with other oligarchs. Once chaotic growth begins, oligarchs safely grow into terrestrial planets.

As chaotic growth ends, several factors probably prevent terrestrial planets from migrating through the remnants of the gaseous disk or the sea of leftover planetesimals. In published simulations, leftover planetesimals have very large e and i (Raymond et al. 2005; Kenyon & Bromley 2006; O’Brien et al. 2006; Raymond et al. 2009b); thus, planets can sweep up or scatter the leftovers faster than they can migrate through them. For typical disk lifetimes of 1–3 Myr, the reduced surface density lowers migration rates through the gas by factors of 10 or more. Migration times are then longer than the disk lifetime, saving terrestrial planets from type I migration through the gas.

Formation outcomes for gas giant planets are less clear. In our picture, isolated oligarchs at 5–10 AU will migrate little through a sea of leftover planetesimals. As chaotic growth begins, these objects start to experience type I migration through the gas. The relative importance of chaotic growth and migration then depends on several factors.

1. *The masses of leftover planetesimals.* Although oligarchs with gaseous atmospheres accrete small planetesimals rapidly (Inaba & Ikoma 2003; Chambers 2006a; Bromley & Kenyon 2011), they cannot accrete large planetesimals on timescales shorter than the migration time (e.g., Chambers 2006b, 2008). Collisional grinding can reduce the sizes of large planetesimals, enabling rapid accretion and the formation of 5–10 M_\oplus cores on very short timescales (Kenyon & Bromley 2009). Thus, rapid core formation depends on the evolution of the size distribution of planetesimals during oligarchic and chaotic growth.
2. *The response of the disk to tightly packed oligarchs.* When oligarchs are tightly packed, their Lindblad resonances overlap. By analogy with our calculations of migration through a sea of planetesimals, we speculate that tightly packed oligarchs cannot migrate. However, there is no analytic or numerical study of type I migration in gaseous disks with tightly packed oligarchs. If tightly packed oligarchs migrate at the “standard” type I rate, then they migrate faster than they grow. If tightly packed oligarchs (and leftover planetesimals) reduce the type I migration rate, then they probably grow faster than they migrate.
3. *The response of the disk to planets accreting gas.* Once planets reach masses of 1–10 M_\oplus , they begin to accrete material from the disk (Mizuno 1980; Stevenson 1982; Ikoma et al. 2000; Rafikov 2006; Hori & Ikoma 2010). At 5 AU, the nominal migration timescale for 10 M_\oplus planets is $\sim 5 \times 10^4 \text{ yr}$, shorter than the accretion timescale of $\gtrsim 10^5 \text{ yr}$ (Pollack et al. 1996; Bodenheimer et al. 2000; Kornet et al. 2002; Papaloizou et al. 2007; Bromley & Kenyon 2011). However, this planet may not migrate so quickly.

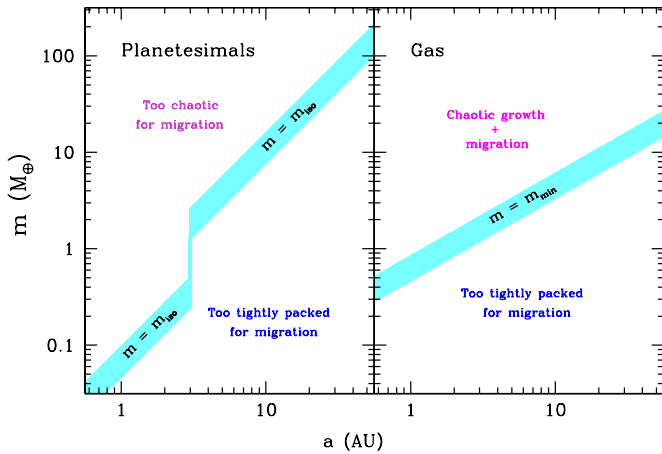


Figure 12. Migration in gaseous and planetesimal disks. In a planetesimal disk (left panel), planets with $m < m_{\text{iso}}$ are packed too closely to migrate. When $m > m_{\text{iso}}$, chaotic growth dominates migration. In a gaseous disk (right panel), planets are spaced too closely to migrate when $m < m_{\text{min}}$. Once $m > m_{\text{min}}$, planets grow chaotically as they migrate. The relative importance of chaotic growth and migration probably depends on the response of the disk to smaller oligarchs and leftover planetesimals.

(A color version of this figure is available in the online journal.)

When the size of the corotation zone is comparable to the disk scale height, the disk may not be able to launch coherent density waves for type I migration. If corotation torques are important, migration may stall until the planet reaches larger masses, forms a gap in the disk, and begins type II migration (Masset et al. 2006).

4. DISCUSSION

Figure 12 summarizes the main conclusions of our analysis. When planets grow in a planetesimal disk (left panel), interactions between closely packed oligarchs ($m < m_{\text{iso}}$) or between chaotic oligarchs ($m > m_{\text{iso}}$) limit migration through a sea of planetesimals. Thus, the building blocks of terrestrial planets and ice or gas giant planets are safe from this form of migration.

In a gaseous disk (right panel), we speculate that low-mass planets ($m < m_{\text{min}}$) are packed too closely to undergo type I migration. If this constraint is correct, the building blocks of terrestrial planets rarely undergo type I migration. Once they are fully formed, terrestrial planets can migrate through the disk. However, the reduced surface density of the disk then limits migration to small radial distances.

Even with these constraints, type I migration is still an issue for the building blocks of gas giant planets. At 5–10 AU, gas giant planet formation depends on the relative importance of migration and chaotic growth. If chaotic growth dominates, the cores of gas giants can form before they migrate. If migration dominates, planets must accrete enough material to begin to accrete gas before they migrate into the central star.

Improving these conclusions requires a better understanding of the transition from oligarchic growth to chaotic growth. During the early stages of oligarchic growth, oligarchs are closely packed within a fairly uniform sea of stirred up planetesimals embedded in a fairly uniform gaseous disk. As oligarchs grow, they become more and more isolated. As they become isolated, oligarchs push the excited planetesimals out of their orbits (e.g., Rafikov 2001). This evolution creates two types of density perturbations within the disk.

1. At the onset of chaotic growth, closely packed oligarchs contain roughly 50% of the mass of solids. These oligarchs create point-like density enhancements in the surface density distribution of the solids.
2. Planetesimals contain the other half of the solid material in the disk. Planetesimals tend to concentrate in rings between the orbits of the oligarchs.

Thus, the surface density distribution of the solids is fairly rippled, with planetesimals concentrated in the peaks of the ripples and oligarchs orbiting within the troughs of the ripples.

Current theory addresses the response of the gaseous disk to isolated oligarchs. For a standard viscous disk, analytic results and numerical simulations yield reasonably robust solutions to the structure of a gaseous disk with an ensemble of widely spaced oligarchs (e.g., Papaloizou et al. 2007; Cresswell & Nelson 2008; Lubow & Ida 2010). Despite many remaining uncertainties in treating the (thermo)dynamics of the gas, the eccentricity of the oligarchs, magnetic fields, turbulence, and other phenomena, interactions between isolated oligarchs and the disk clearly lead to migration.

Although the planetesimal theory predicts ensembles of closely packed oligarchs, migration theory does not address the structure of the gaseous disk at the onset of chaotic growth. Closely packed oligarchs clearly cannot migrate through a planetesimal disk (Figure 7). We speculate that overlapping Lindblad resonances prevent migration through a gaseous disk. New analytic and numerical approaches are required to test this idea.

Migration theory also does not include the response of the disk to the ensemble of leftover planetesimals. Analytic solutions suggest that oligarchs create gaps in the surface density distribution of planetesimals (Rafikov 2001). Many numerical simulations show that growing oligarchs push away and scatter leftover planetesimals (e.g., Malhotra 1993; Kokubo & Ida 1998; Morbidelli et al. 2008; Kirsh et al. 2009, and references therein). With $\sim 50\%$ of the solid mass at the onset of chaotic growth, structure in the spatial distribution of planetesimals probably leads to density waves within the gas. Density waves from individual planetesimals probably have negligible impact on oligarchs or planetesimals. However, density waves from the ensemble of planetesimals can interact with oligarchs orbiting several r_H away. It is not clear whether this interaction impacts migration significantly; however, including the behavior of planetesimals is necessary for a complete theory of migration through a gaseous disk.

Addressing the response of the disk to closely packed oligarchs and to leftover planetesimals will improve our understanding of planet formation. Despite our good working knowledge of the growth of oligarchs from planetesimals (e.g., Wetherill & Stewart 1993; Kenyon & Bromley 2008, 2010), the formation of planetesimals (e.g., Youdin 2010), the transition from oligarchy to chaos (e.g., Goldreich et al. 2004; Kenyon & Bromley 2006), and the long-term evolution of fully formed planets within a gaseous disk (e.g., Ida & Lin 2005; Papaloizou et al. 2007; Lubow & Ida 2010) are less robust aspects of the theory. Complete numerical simulations of migration with a gaseous disk, closely packed oligarchs, and a sea of leftover planetesimals are beyond the capabilities of current computers. Smaller simulations of disks with rings of planetesimals and a few oligarchs are possible and would begin to address how planetesimals might change migration rates through the disk.

5. SUMMARY

We have used analytic results and numerical simulations to explore aspects of migration in protostellar disks.

1. We derive “universal” rates for isolated planets migrating rapidly, Equation (13), or slowly, Equation (14), through a disk of planetesimals. When the mass of the planet is much much smaller than the mass of the central star, these rates agree with comprehensive numerical simulations and with rates derived from previous studies (e.g., Ida et al. 2000; Levison et al. 2007; Kirsh et al. 2009; Bromley & Kenyon 2011). We derive an upper limit m_{fast} (Equation (10)) on the mass of a rapidly migrating planet. In a disk with surface density $\Sigma = 30 \text{ g cm}^{-2}$ at $a = 1 \text{ AU}$, $m_{\text{fast}} \approx 0.025 M_{\oplus}$; for $\Sigma \propto a^{-1}$, $m_{\text{fast}} \propto a^{-3}$. When $m > m_{\text{fast}}$, fast migration rates are inversely proportional to the mass of the planet (Figure 3). This result is new.
2. Tests of planets migrating through a disk of stirred up planetesimals verify that rates scale with the eccentricity of background planetesimals in Hill units, e_{H}^{-3} (Figure 4; see also Ida et al. 2000; Kirsh et al. 2009).
3. The strong scaling with e_{H} suggests that planets cannot migrate through the wakes of stirred up planetesimals left behind by another migrating planet. Several tests confirm this hypothesis (Figures 5–7). Thus, closely packed oligarchs do not migrate. This result is also new.
4. When a newly formed planet migrates or is scattered into a region where planetesimals have small e_{H} , this isolated planet can migrate through a large part of the disk (see also Malhotra 1993; Levison et al. 2007).

We use some simple arguments to generalize these results to migration through a gaseous disk.

1. Adopting the disk scale height h as the scale for density perturbations in the disk, we show that rates for type I, type II (in the zero viscosity limit), and type III migration through gaseous disks are similar in magnitude and scaling to rates through planetesimal disks.
2. If closely packed oligarchs migrate as poorly through gaseous disks as they migrate through planetesimal disks, we derive limits on the masses of oligarchs that undergo type I migration through disks with surface density $\Sigma = \Sigma_0 a^{-1}$.

Combining these results into a single diagram (Figure 12), we conclude that type I migration is an important issue during the formation of gas giant planets. The building blocks of these planets are probably safe until they reach the isolation mass (m_{iso} ; Equation (26)). Once their masses exceed m_{iso} , the migration rate depends on how the gas responds to the mass distribution of smaller oligarchs and leftover planetesimals. Addressing this issue requires new analyses.

For terrestrial planets, we conclude that type I migration is unimportant. Throughout oligarchic and chaotic growth, the building blocks of rocky planets are packed too closely to migrate. Once these planets are fully formed, the surface density of the gas is probably too low to support type I migration. Thus, our analysis suggests that standard calculations of terrestrial planet formation without migration yield robust estimates of the formation timescale and orbital properties of terrestrial planets.

Advice and comments from M. Duncan, M. Geller, D. Kirsh, S. Tremaine, A. Youdin, and the anonymous referee greatly improved our presentation. Portions of this project were

supported by NASA’s *Astrophysics Theory Program*, and the *Origin of Solar Systems Program* through grant NNX10AF35G.

REFERENCES

- Adams, F. C., & Bloch, A. M. 2009, *ApJ*, 701, 1381
 Alexander, R. D., & Armitage, P. J. 2009, *ApJ*, 704, 989
 Alibert, Y., Mordasini, C., & Benz, W. 2004, *A&A*, 417, L25
 Andrews, S. M., & Williams, J. P. 2007, *ApJ*, 671, 1800
 Armitage, P. J. 2007, *ApJ*, 665, 1381
 Artymowicz, P. 1993a, *ApJ*, 419, 155
 Artymowicz, P. 1993b, *ApJ*, 419, 166
 Artymowicz, P. 1997, *Annu. Rev. Earth Planet. Sci.*, 25, 175
 Artymowicz, P. 2004, in ASP Conf. Ser. 324, *Debris Disks and the Formation of Planets*, ed. L. Caroff et al. (San Francisco, CA: ASP), 39
 Bate, M. R., Lubow, S. H., Ogilvie, G. I., & Miller, K. A. 2003, *MNRAS*, 341, 213
 Bodenheimer, P., Hubickyj, O., & Lissauer, J. J. 2000, *Icarus*, 143, 2
 Bromley, B. C., & Kenyon, S. J. 2006, *AJ*, 131, 2737
 Bromley, B. C., & Kenyon, S. J. 2011, *ApJ*, 731, 101
 Bryden, G., Chen, X., Lin, D. N. C., Nelson, R. P., & Papaloizou, J. C. B. 1999, *ApJ*, 514, 344
 Chambers, J. 2006a, *Icarus*, 180, 496
 Chambers, J. 2008, *Icarus*, 198, 256
 Chambers, J. E. 2006b, *ApJ*, 652, L133
 Chatterjee, S., Ford, E. B., & Rasio, F. A. 2010, arXiv:1012.0584
 Chiang, E. I., & Goldreich, P. 1997, *ApJ*, 490, 368
 Chiang, E., & Youdin, A. N. 2010, *Annu. Rev. Earth Planet. Sci.*, 38, 493
 Cresswell, P., & Nelson, R. P. 2006, *A&A*, 450, 833
 Cresswell, P., & Nelson, R. P. 2008, *A&A*, 482, 677
 Crida, A., Masset, F., & Morbidelli, A. 2009, *ApJ*, 705, L148
 Crida, A., Morbidelli, A., & Masset, F. 2006, *Icarus*, 181, 587
 Crida, A., Papaloizou, J. C. B., Rein, H., Charnoz, S., & Salmon, J. 2010, *AJ*, 140, 944
 Currie, T., Lada, C. J., Plavchan, P., Robitaille, T. P., Irwin, J., & Kenyon, S. J. 2009, *ApJ*, 698, 1
 D’Angelo, G., Bate, M. R., & Lubow, S. H. 2005, *MNRAS*, 358, 316
 D’Angelo, G., Durisen, R. H., & Lissauer, J. J. 2010, in *Exoplanets*, ed. S. Seager (Tucson, AZ: Univ. Arizona Press), 319
 D’Angelo, G., Henning, T., & Kley, W. 2003, *ApJ*, 599, 548
 D’Angelo, G., & Lubow, S. H. 2008, *ApJ*, 685, 560
 D’Angelo, G., & Lubow, S. H. 2010, *ApJ*, 724, 730
 Dermott, S. F., & Murray, C. D. 1981, *Icarus*, 48, 1
 Edgar, R., & Artymowicz, P. 2004, *MNRAS*, 354, 769
 Gladman, B. 1993, *Icarus*, 106, 247
 Goldreich, P., Lithwick, Y., & Sari, R. 2004, *ARA&A*, 42, 549
 Goldreich, P., & Tremaine, S. 1979, *ApJ*, 233, 857
 Goldreich, P., & Tremaine, S. 1980, *ApJ*, 241, 425
 Hahn, J. M., & Malhotra, R. 1999, *AJ*, 117, 3041
 Haisch, K. E., Jr., Lada, E. A., & Lada, C. J. 2001, *ApJ*, 553, L153
 Hayashi, C. 1981, *Prog. Theor. Phys. Suppl.*, 70, 35
 Hori, Y., & Ikoma, M. 2010, *ApJ*, 714, 1343
 Ida, S., Bryden, G., Lin, D. N. C., & Tanaka, H. 2000, *ApJ*, 534, 428
 Ida, S., & Lin, D. N. C. 2004, *ApJ*, 604, 388
 Ida, S., & Lin, D. N. C. 2005, *ApJ*, 626, 1045
 Ida, S., & Lin, D. N. C. 2008, *ApJ*, 673, 487
 Ikoma, M., Nakazawa, K., & Emori, H. 2000, *ApJ*, 537, 1013
 Inaba, S., & Ikoma, M. 2003, *A&A*, 410, 711
 Isella, A., Carpenter, J. M., & Sargent, A. I. 2009, *ApJ*, 701, 260
 Kennedy, G. M., & Kenyon, S. J. 2008, *ApJ*, 673, 502
 Kennedy, G. M., & Kenyon, S. J. 2009, *ApJ*, 695, 1210
 Kenyon, S. J., & Bromley, B. C. 2001, *AJ*, 121, 538
 Kenyon, S. J., & Bromley, B. C. 2002, *AJ*, 123, 1757
 Kenyon, S. J., & Bromley, B. C. 2004, *AJ*, 127, 513
 Kenyon, S. J., & Bromley, B. C. 2006, *AJ*, 131, 1837
 Kenyon, S. J., & Bromley, B. C. 2008, *ApJS*, 179, 451
 Kenyon, S. J., & Bromley, B. C. 2009, *ApJ*, 690, L140
 Kenyon, S. J., & Bromley, B. C. 2010, *ApJS*, 188, 242
 Kenyon, S. J., & Hartmann, L. 1987, *ApJ*, 323, 714
 Kenyon, S. J., & Luu, J. X. 1998, *AJ*, 115, 2136
 Kirsh, D. R., Duncan, M., Brassier, R., & Levison, H. F. 2009, *Icarus*, 199, 197
 Klahr, H., & Kley, W. 2006, *A&A*, 445, 747
 Kley, W., Bitsch, B., & Klahr, H. 2009, *A&A*, 506, 971
 Kley, W., & Crida, A. 2008, *A&A*, 487, L9
 Kokubo, E., & Ida, S. 1998, *Icarus*, 131, 171
 Kokubo, E., & Ida, S. 2000, *Icarus*, 143, 15

- Kokubo, E., & Ida, S. 2002, *ApJ*, **581**, 666
- Kornet, K., Bodenheimer, P., & Różyczka, M. 2002, *A&A*, **396**, 977
- Levison, H. F., Morbidelli, A., Gomes, R., & Backman, D. 2007, in *Protostars and Planets V*, ed. B. Reipurth, D. Jewitt, & K. Keil (Tucson, AZ: Univ. Arizona Press), 669
- Lin, D. N. C., Bodenheimer, P., & Richardson, D. C. 1996, *Nature*, **380**, 606
- Lin, D. N. C., & Papaloizou, J. 1979, *MNRAS*, **186**, 799
- Lin, D. N. C., & Papaloizou, J. 1986, *ApJ*, **309**, 846
- Lin, D. N. C., & Papaloizou, J. C. B. 1993, in *Protostars and Planets III*, ed. E. H. Levy & J. I. Lunine (Tucson, AZ: Univ. Arizona Press), 749
- Lissauer, J. J. 1987, *Icarus*, **69**, 249
- Lubow, S. H., & Ida, S. 2010, in *Exoplanets*, ed. S. Seager (Tucson, AZ: Univ. Arizona Press), 347
- Malhotra, R. 1993, *Nature*, **365**, 819
- Mamajek, E. E. 2009, in *AIP Conf. Proc.* 1158, *Exoplanets and Disks: Their Formation and Diversity*, ed. T. Usada, M. Tamura, & M. Ishii (Melville, NY: AIP), 3
- Martin, R. G., Lubow, S. H., Pringle, J. E., & Wyatt, M. C. 2007, *MNRAS*, **378**, 1589
- Marzari, F., & Weidenschilling, S. J. 2002, *Icarus*, **156**, 570
- Masset, F. S., D'Angelo, G., & Kley, W. 2006, *ApJ*, **652**, 730
- Masset, F. S., & Papaloizou, J. C. B. 2003, *ApJ*, **588**, 494
- Mizuno, H. 1980, *Prog. Theor. Phys.*, **64**, 544
- Morbidelli, A., Levison, H. F., & Gomes, R. 2008, in *The Solar System Beyond Neptune*, ed. M. A. Barucci et al. (Tucson, AZ: Univ. Arizona Press), 275
- Mordasini, C., Alibert, Y., Benz, W., & Naef, D. 2009, *A&A*, **501**, 1161
- Nelson, R. P., & Papaloizou, J. C. B. 2004, *MNRAS*, **350**, 849
- O'Brien, D. P., Morbidelli, A., & Levison, H. F. 2006, *Icarus*, **184**, 39
- Ormel, C. W., & Klahr, H. H. 2010, *A&A*, **520**, A43
- Paardekooper, S.-J., Baruteau, C., Crida, A., & Kley, W. 2010, *MNRAS*, **401**, 1950
- Paardekooper, S.-J., Baruteau, C., & Kley, W. 2011, *MNRAS*, **410**, 293
- Paardekooper, S.-J., & Mellema, G. 2006a, *A&A*, **450**, 1203
- Paardekooper, S.-J., & Mellema, G. 2006b, *A&A*, **459**, L17
- Paardekooper, S.-J., & Papaloizou, J. C. B. 2008, *A&A*, **485**, 877
- Paardekooper, S.-J., & Papaloizou, J. C. B. 2009a, *MNRAS*, **394**, 2283
- Paardekooper, S.-J., & Papaloizou, J. C. B. 2009b, *MNRAS*, **394**, 2297
- Papaloizou, J. C. B., & Larwood, J. D. 2000, *MNRAS*, **315**, 823
- Papaloizou, J. C. B., Nelson, R. P., Kley, W., Masset, F. S., & Artymowicz, P. 2007, in *Protostars and Planets V*, ed. B. Reipurth, D. Jewitt, & K. Keil (Tucson, AZ: Univ. Arizona Press), 655
- Pepliński, A., Artymowicz, P., & Mellema, G. 2008a, *MNRAS*, **386**, 164
- Pepliński, A., Artymowicz, P., & Mellema, G. 2008b, *MNRAS*, **386**, 179
- Pollack, J. B., Hubickyj, O., Bodenheimer, P., Lissauer, J. J., Podolak, M., & Greenzweig, Y. 1996, *Icarus*, **124**, 62
- Pringle, J. E. 1981, *ARA&A*, **19**, 137
- Rafikov, R. R. 2001, *AJ*, **122**, 2713
- Rafikov, R. R. 2006, *ApJ*, **648**, 666
- Raymond, S. N., Armitage, P. J., & Gorelick, N. 2009a, *ApJ*, **699**, L88
- Raymond, S. N., Armitage, P. J., & Gorelick, N. 2010, *ApJ*, **711**, 772
- Raymond, S. N., O'Brien, D. P., Morbidelli, A., & Kaib, N. A. 2009b, *Icarus*, **203**, 644
- Raymond, S. N., Quinn, T., & Lunine, J. I. 2005, *ApJ*, **632**, 670
- Stevenson, D. J. 1982, *Planet. Space Sci.*, **30**, 755
- Tanaka, H., Takeuchi, T., & Ward, W. R. 2002, *ApJ*, **565**, 1257
- Terquem, C. E. J. M. L. J. 2003, *MNRAS*, **341**, 1157
- Thommes, E. W., Duncan, M. J., & Levison, H. F. 2002, *AJ*, **123**, 2862
- Thommes, E. W., Matsumura, S., & Rasio, F. A. 2008, *Science*, **321**, 814
- Tsiganis, K., Gomes, R., Morbidelli, A., & Levison, H. F. 2005, *Nature*, **435**, 459
- Veras, D., Crepp, J. R., & Ford, E. B. 2009, *ApJ*, **696**, 1600
- Ward, W. R. 1991, *Lunar and Planetary Inst. Sci. Conf. Abstracts*, **22**, 1463
- Ward, W. R. 1997, *Icarus*, **126**, 261
- Weidenschilling, S. J. 1977, *Ap&SS*, **51**, 153
- Wetherill, G. W., & Stewart, G. R. 1993, *Icarus*, **106**, 190
- Williams, J. P., & Cieza, L. A. 2011, arXiv:1103.0556
- Wyatt, M. C. 2003, *ApJ*, **598**, 1321
- Wyatt, M. C., Greaves, J. S., Dent, W. R. F., & Coulson, I. M. 2005, *ApJ*, **620**, 492
- Youdin, A. N. 2010, *EAS Publ. Ser.*, **41**, 187
- Youdin, A. N., & Lithwick, Y. 2007, *Icarus*, **192**, 588